Journal of Medicinal Chemistry

Article

pubs.acs.org/jmc

A Small Nonrule of 3 Compatible Fragment Library Provides High Hit Rate of Endothiapepsin Crystal Structures with Various Fragment Chemotypes†

Helene Köster,[‡,#] Tobias Craan,[‡,#] Sascha Brass,[‡] Christian Herhaus,[§] Matthias Zentgraf,[∥] Lars Neumann,[⊥] Andreas Heine,[‡] and Gerhard Klebe*[,‡]

[‡]Department of Pharmaceutical Chemistry, Philipps University Marburg, Marbacher Weg 6, 35032 Marburg, Germany

[§]Merck KGaA, Frankfurter Straße 250, 64293 Darmstadt, Germany

[∥]Boehringer Ingelheim Pharma GmbH & Co. KG, Birkendorfer Straße 65, 88397 Biberach/Riß, Germany

[⊥]Proteros Biostructures, Bunsenstr. 7a, D-82152 Martinsried, Germany

ABSTRACT: Druglike molecules are defined by Lipinski's rule of 5, to characterize fragment thresholds, they have been reduced from 5 to 3 (Astex's rule of 3). They are applied to assemble fragment libraries, and providers use them to select fragments for commercial offer. We question whether these rules are too stringent to compose fragment libraries with candidates exhibiting sufficient room for chemical subsequent growing and merging modifications as appropriate functional groups for chemical transformations are required. Usually these groups exhibit properties as hydrogen bond donors/acceptors and provide entry points for optimization chemistry. We therefore designed a fragment library (364 entries) without strictly applying the rule of 3. For initial screening for endothiapepsin binding, we performed a biochemical cleavage assay of a fluorogenic substrate at 1 mM. "Hits" were defined to inhibit the enzyme by at least 40%. Fifty-five hits were suggested and subsequently soaked into endothiapepsin crystals. Eleven crystal structures could be determined covering fragments with diverse binding modes: (i) direct binding to the catalytic dyad aspartates, (ii) water-mediated binding to the aspartates, (iii) no direct interaction with the dyad. They occupy different specificity pockets. Only 4 of the 11 fragments are consistent with the rule of 3. Restriction to this rule would have limited the fragment hits to a strongly reduced variety of chemotypes.

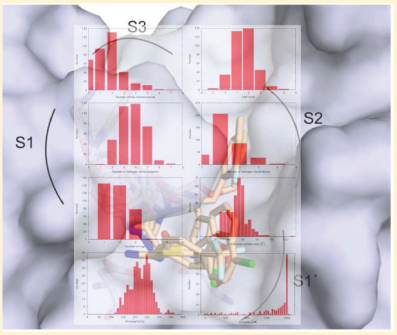

INTRODUCTION

The steadily increasing disclosure of novel and interesting target structures for therapeutic intervention, often stimulated by results from proteomics and structural genomics, increasingly demands efficient strategies to discover first leads to interfere with protein function. In the 1990s high-throughput screening and combinatorial chemistry have been established to resolve the bottleneck for an efficient lead discovery. Subsequently, virtual computer screening has been added as an alternative to complement these approaches. However, success rates were not as expected and the size of the discovered hits was in the range of common drug molecules not leaving much space for optimization without significantly exceeding the molecular weight limit of about 500 g/mol.[1] To better evaluate the size of a discovered hit with respect to its achieved potency, the concept of ligand efficiency[2] was introduced. Highly efficient leads exhibit good potency combined with low molecular weight.

Advances in biophysical techniques to detect protein−ligand binding and increasing success to acquire structural information about protein−ligand complexes by crystallography[3−5] or NMR spectroscopy[6−8] allowed the pushing of the limits of the compounds to be screened to lower molecular weight. Particularly NMR and surface plasmon resonance (SPR) are nowadays supposed to be reliable enough to detect very small and weak binders which exhibit sufficient and convincing potency ("high" ligand efficiency).[2] Other approaches intend to screen directly with proteins in crystalline state.[5,9] Fragment-type[10] leads appear as a special challenge, as they provide (once characterized in terms of a crystal structure) wide opportunities for optimization into prospective drug candidates. Many examples have meanwhile been described in the literature, and an impressive number of reviews have been written,[11−22] mostly developed in industry or specialized small biotechnology companies along the following targets: HSP90,[23−28] different kinases,[29−36] phosphatases,[37−39] antibacterial and anti-infective targets,[40−44] BCL-2,[45] and BACE.[45−48]

Druglike molecules are usually defined by Lipinski's rules ("RO5").[1] This "rule of 5" tries to summarize properties that are needed to achieve oral availability which is essential for an active substance as prospective candidate for clinical trials. Similar rules have been defined for fragments and became popular as Astex's "rule of 3" ("RO3").[10] These rules reduce the various thresholds from 5 to 3. In particular, the crucial molecular weight is <300 g/mol, the number of hydrogen bond

Received: May 19, 2011
Published: October 6, 2011

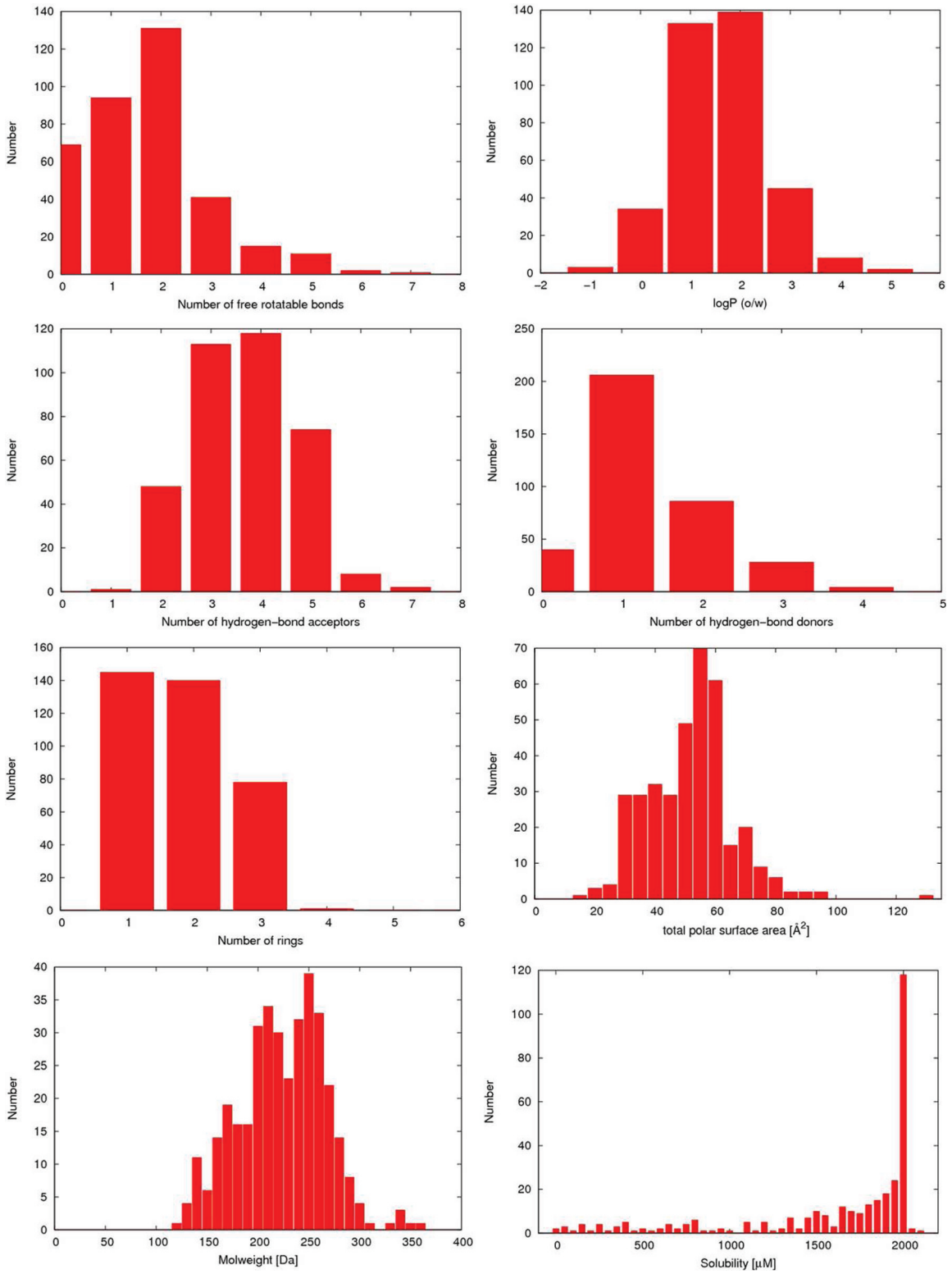

Figure 1. Distribution of physicochemical and structural properties across the library entries.

donors and acceptors is ≤3, XlogP is ≤3,[10] the number of freely rotatable bonds is ≤3, and the polar surface area is ≤60 Å^2. As a consequence, for fragment libraries assembled and offered commercially, many providers over the past years try to stick to these rules and select the fragments that largely conform with Astex's "RO3".

In this contribution, we critically ask whether these rules are too stringent for a fragment library holding candidates that leave sufficient room for subsequent chemical modifications. In terms of strategies focusing on fragment growing and fragment merging, an appropriate number of functional groups is required. Frequently, these groups display properties as hydrogen donors and/or hydrogen acceptors. They can be

dx.doi.org/10.1021/jm200642w | J. Med. Chem. 2011, 54, 7784–7796

used also as synthetic handles to start the required optimization chemistry. Therefore, we designed a small fragment library without adhering strictly to the RO3 criteria for fragments but that should be well suited for crystallographic screening and follow-up chemistry. Subsequently, we screened endothiapepsin with this library. Besides finding new fragment binders for this protease and their crystallographic characterization, we were interested to find out how well the discovered fragments agree with the Astex's "RO3".

Endothiapepsin serves as a model system for the large group of pepsin-like aspartic proteases. In this family there are many proteins that are involved in serious diseases such as malaria (plasmepsins), fungal infections (secreted aspartic proteinases), Alzheimer's disease (β-secreatase), and hypertension (renin). In the 1980s this protein was the working horse for the development of blood pressure depressions before the crystal structure of renin became available. This emphasizes the relevance of endothiapepsin as a suitable reference protein. In the past it has already been successfully used as a model system by others. Here, it provided important information for understanding the details of the catalytic mechanism[49] as well as developing renin inhibitors.[50] Endothiapepsin was also a successful model in discovering novel fragments binding to β-secretase.[51]

RESULTS

Library Design. Initially, we asked several chemical suppliers (ASINEX, ChemBridge, MayBridge, InterBio Screen, LifeChemicals, Enamine, Specs, Vitas M Laboratory) to name their commercially offered compounds with ≤20 non-hydrogen atoms, including only C, N, O, F, Cl, Br, P and an availability of at least 100 mg. In spring 2009, this resulted in 238 224 compounds. Since the library was intended to be screened crystallographically, fragments containing strong X-ray scatterers such as bromine were considered advantageous. Because of the high molecular weight of such electron rich atoms, we restricted the size of our fragments by the number of non-hydrogen atoms instead of molecular weight. Thus, we defined the fragments to have between 8 and 20 non-hydrogen atoms. The range of the molecular weight in the final library is between 122 and 359 g/mol with an average of 224 g/mol (Figure 1, Table 1).

Table 1. Physicochemical Parameters of the Library

parameter	min	max	average
no. of heavy atoms	8	20	15
MW [g/mol]	122	359	224
Lipinski donor	0	4	1.3
Lipinski acceptor	1	7	3,7
log P	−1.3	5.4	1.6
free rotabtable bonds	0	7	1.7
TPSA (Å^2)	15	126	52

Next we filtered for particular functional groups to discard potentially toxic, unwanted, or chemically unstable moieties. The applied filters are similar to those developed by Baurin and colleagues at Vernalis.[52]

All physicochemical properties have been calculated under the assumption of standard protonation states at physiological pH conditions using MOE.[53] Rotatable bonds were not restrained (Figure 1). Therefore, the number of rotatable bonds in the final database varies from 0 to 7 with an overall average of 1.7 (Table 1). The log P value was calculated within the MOE software (clogP(o/w))[53]and was filtered to be ≤3. For particular chemical motifs the threshold was expanded to 5.4 (Figure 1). Thus, the calculated lipophilicity spreads from −1.25 to 5.39 with a mean of 1.58 (Table 1).

For hydrogen-bond acceptors we filtered differently from the "RO3" to be more comparable to the "RO5" criteria.[1] There the number of hydrogen-bond acceptors is multiplied by a factor of 2 considering 10 hydrogen-bond acceptors as appropriate. Transferring this factor to the "RO3" for fragments, six hydrogen-bond acceptors are acceptable. In special cases only, we allowed fragments to exceed this number of hydrogen-bond acceptors as upper limit (Figure 1). In the final fragment library the hydrogen-bond acceptor range falls between 1 and 7 with an average of 3.7. The hydrogen-bond donors have been selected to be in agreement with the original "RO3". Only a few chemical scaffolds had a larger number of hydrogen-bond donors so that this property finally varied from 0 to 4 with an average of 1.3. For the total polar surface area (TPSA) we increased the threshold from 60 to 80 Å^2. Again, we allowed some chemotypes to deviate from this upper threshold. In the final library the TPSA ranged between 15 and 126 Å^2 with a mean of 52 Å^2.

The filtered fragments were clustered, manually prioritized, and selected by visual inspection to avoid strong accumulation of similar chemotypes and to cover a sufficient range of deviating chemical scaffolds. Every entry was requested to contain at least one ring system. The overwhelming majority shows one or two ring systems (frequently fused) and about 20% with three ring systems.

Considering in detail the finally selected 364 compounds of our library, 141 fragments conform to the "RO3" whereas 223 fragments do not agree with the respective criteria. In terms of stereochemistry, 55 compounds comprise at least one stereogenic center. For chiral compounds usually the racemates have been purchased. Finally, experimental solubility was determined to be >1 mM for 76% of the compounds (Figure 1). Considering upper and lower threshold limits of the "RO3", we exceeded the ranges of all considered rules, but with respect to the average values our selection fell well into the limitation of the rules. Only the average number of acceptors was clearly beyond the range set by the original "RO3". Purity of the compounds was checked, and apart from 22 entries sufficient purity could be registered.

Validating the Library on Endothiapepsin. To validate the suitability of our library for fragment screening purposes, all entries were tested against endothiapepsin in a fluorescence-based competition assay. All compounds were screened at 1 mmol/L concentration. Due to insufficient solubility under the applied assay conditions 14 fragments were excluded and another 18 compounds could only be screened at 500 μmol/L. Finally, 17 entries were excluded from the assay screen because of self-fluorescence.

For the screen, the hit criterion was set to at least 40% inhibition of protein function, suggesting 55 entries to enter a subsequent crystallographic screen. The fragments were soaked into native endothiapepsin crystals in mixtures of two compounds. Principally, screening cocktails of several fragments at a time speeds up the search and provides the chance to discover cooperative binding. However, simultaneous soaking of multiple compounds enhances the risk of competition for the same binding site and will reduce the maximally possible ligand concentration in the mother liquid.

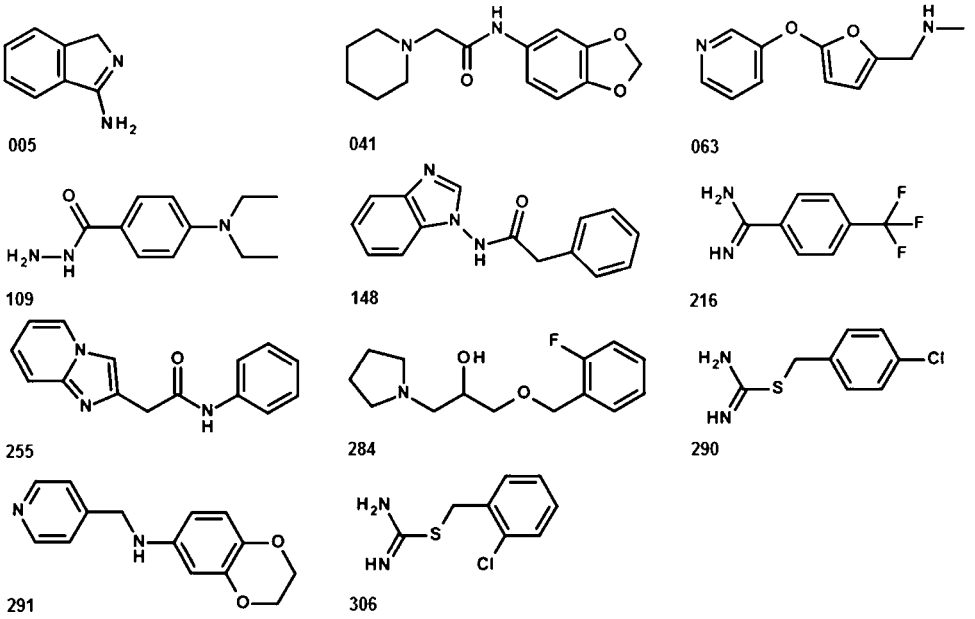

Figure 2. Chemical formulas of the 11 hits that successfully provided complexes in crystal structure analysis.

We therefore decided to use mixtures of only two compounds, as we expected the overwhelming part of fragments to interact with the catalytic dyad. In this case, one compound of such a mixture was identified in a crystal structure; the other one was soaked again in a different cocktail. Simultaneous binding of two fragments was never observed.

In total, 11 crystal structures were obtained (Figure 2). The hit rate of the fluorescence-based assay with 55 hits out of a 364 membered fragment library is remarkably high. The observed 11 crystal structures out of the initially detected 55 hits suggest that the composition of our assembled fragment library is efficiently done and the complete initial screening based on the fluorescence-based assay was a good filter.

Table 2 shows the assay results. The inhibition of endothiapepsin ranges from 42% to 100%. The 40% inhibition was set as threshold to accept a test candidate as "hit". The 11 fragments of which we could determine a crystal structure are highlighted. The % inhibition does not correlate with the probability of penetrating into the crystals and successfully revealing a crystal structure. Interestingly enough, we were not able to successfully determine crystal structures of the eight fragments, suggesting full inhibition in the fluorescence-based assay; however, we were able to crystallize fragments with the enzyme that displayed less than 50% inhibition.

To find meaningful parameters that correlate with successful crystal soaking and structure determination, we closely examined the crystallographically characterized fragments. Table 3 lists the physicochemical parameters of these fragments. The molecular weight ranges from 168 to 262 g/mol, which is in agreement with the Astex rules. All 11 fragments have between one and three donors. Remarkably, the hydrogen-bond acceptors show a different picture. Six out of the 11 hits possess four or more acceptors. Only five compounds exhibit between one and three acceptors, the number principally allowed by the "RO3". Therefore, with respect to the latter criterion, most of our discovered fragments do not meet the Astex rules. Interestingly, 6 of the 11 hits involve all their hydrogen-bond acceptors interacting with the protein. The log P is in most cases below 3 and agrees with

Table 2. Summary of the Screening Results[a]

fragment	% inhibition	fragment	% inhibition	fragment	% inhibition
149	100	**297**	78	**201**	51
177	100*	**186**	76	**065**	50
178	100	**333**	76	***291***	*50*
236	100	**175**	75	***041***	*49*
238	100	**301**	75	**088**	47
042	99	**040**	73	**137**	47
064	99	***063***	*66*	**188**	47
017	97	**252**	64	**261**	47
306	*93*	**224**	63	**051**	46
003	92	**159**	60	**141**	46
168	92	**183**	60	**140**	45
005	*89*	**335**	60	***216***	*45*
083	89	**134**	57	**295**	44
109	*89*	**176**	55	**362**	43
284	*87*	**192**	55*	**171**	42
255	*84*	**266**	54*		
290	*84*	**267**	54		
142	80	**308**	53		
161	80	**222**	52		
093	79	***148***	*51*		

[a]Hits leading to a crystal structure are underlined and in italic font. Values marked with an asterisk are measured at a 500 μmol/L inhibitor; all other were measured at 1 mmol/L.

Astex's "RO3". Only one fragment displays a log P of 3.3 and departs somewhat from these limits. The free rotatable bonds range from 0 to 6. The majority has less than three free rotatable bonds, and only two fragments differ and show four and six rotatable bonds. Thus, the last two fragments infringe on the Astex rules. The total polar surface area is in all cases below 60 Å^2 and thus fully agrees with the limitation set by the rules.

In summary 7 of the 11 fragments that lead to a crystal structure violate at least one parameter of Astex's "RO3".

dx.doi.org/10.1021/jm200642w|J. Med. Chem. 2011, 54, 7784–7796

Table 3. Physicochemical Parameters of the Fragments Detected in a Crystal Structure

fragment	heavy atoms	weight[53] (g/mol)	Lipinski donor[53]	Lipinski acceptor[53]	log P [53]	free rotatable bond	TPSA[53] (Å^2)
005	10	169	2	2	2.2	0	38.4
041	19	262	1	5	1.6	3	50.8
063	15	204	1	4	1.0	4	47.3
109	15	207	3	4	1.0	2	58.4
148	19	251	1	4	2.2	2	46.9
216	13	261	3	2	3.3	1	49.9
255	19	251	1	4	1.8	3	46.9
284	18	253	1	3	2.0	6	32.7
290	12	201	3	2	2.9	2	49.9
291	18	242	1	4	1.7	2	43.4
306	12	201	3	2	2.9	2	49.9

Solubility has been discussed to be a crucial property.[28] To investigate the impact of solubility, we measured the aqueous buffer solubility of our fragments at a pH of 7.4. During library design we applied computer tools[54,55] and property calculations to select fragments with expected high solubility. The most important parameter to predict this property was log P, which varied from −1.25 to 5.39 with an average of 1.58 (Table 1). The measured solubilities are presented in Table 4 and Figure 1. A total of 36 fragments could not be evaluated because of self-fluorescence. 76% of the fragments show solubility greater than 1 mmol/L, indicating a quite successful computational selection procedure. To further characterize the discovered crystallographic hits, we compared the solubility of these compounds with the assay hits and with all entries of the library. As can be seen in Table 4 the solubility of the assay hits varies over the entire solubility range with a slight tendency toward better solubility. All fragments that also penetrate into the crystals show a solubility of greater than 1.5 mmol/L. This observation suggests that better soluble fragments are more likely to show up as an assay hit. With regard to the probability of penetrating into the crystals apart from reasonable inhibition properties, pronounced solubility seems to be an even more important aspect.

Table 4. Solubility Data for Library Entries[a]

	all (364) (%)	hits (55) (%)	structure (11) (%)
ND	10	2	0
0	1	0	0
0−0.5 mM	6	2	0
0.5−1 mM	7	2	0
1−1.5 mM	10	14	0
1.5−2 mM	38	53	64
>2 mM	28	27	36

[a]Second column: all data. Third column: for the 55 initial assay hits. Fourth column: for the 11 fragments providing crystal structures. ND = not detected because of self-fluorescence.

Analysis of the Crystal Structures. Endothiapepsin is secreted by the fungus *Cryphonectria parasitica*. Like most aspartic proteinases the protein is activated in acid medium. After cleavage of the N-terminal propeptide the active protein consists of 330 amino acids with a molecular weight of 34 kDa. The catalytic site consists of two aspartates. While Asp35 is deprotonated, Asp219 is supposed to carry one proton.[49,56] This protonation state is stabilized by the surrounding amino acids.[57] In the uncomplexed state, a water molecule is bound between the two aspartates. During the first step of proteolysis this water molecule is able to attack the scissile bond of a peptide, leading to its cleavage. The active site of the protein is covered by the flap, a highly flexible β-hairpin loop. The catalytic dyad and the most important pockets are shown in Figure 3.

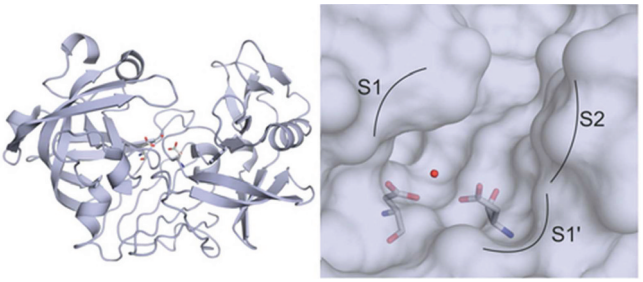

Figure 3. Left: Overall folding structure of endothiapepsin with the catalytic dyad in the center. Right: Blow-up of the uncomplexed binding pocket with the catalytic water and the two catalytic aspartates. The adjacent specificity pockets S1′, S1, and S2′ are indicated on the solvent accessible surface.

Eleven crystal structures of a fragment in complex with endothiapepsin were obtained with resolutions ranging between 1.25 and 1.90 Å. The soaked fragments disclose their binding mode in all complexes by a well-resolved $F_o - F_c$ difference electron density and suggest population of at least 90%. The compounds show diverse binding modes that can be divided into three categories: direct binding to the two catalytic aspartates, binding to the two catalytic aspartates mediated by a water molecule, and no direct interaction with the catalytic dyad.

Direct binding to the two catalytic aspartates could be observed in seven cases, making this the most prominent interaction motif (Figure 4). Fragment **109** addresses the two catalytic aspartates through its terminal nitrogen of the hydrazine carbonyl moiety. The terminal nitrogen interacts with both aspartates, and through a water molecule it is bridging an interaction to Gly37 in the front part of the S1′ pocket. The major part of the ligand skeleton is orientated toward the S1 pocket. The fragment is populated to 90% and shows some disorder concerning the two terminal ethyl substituents (Figure 4). Additionally, a DMSO molecule is bound in the front part of the S4 pocket interacting with Thr223.

Fragment **005** binds to the catalytic dyad with its exocyclic amino group placed between the two aspartates. The endocyclic nitrogen atom of the five-membered ring forms a

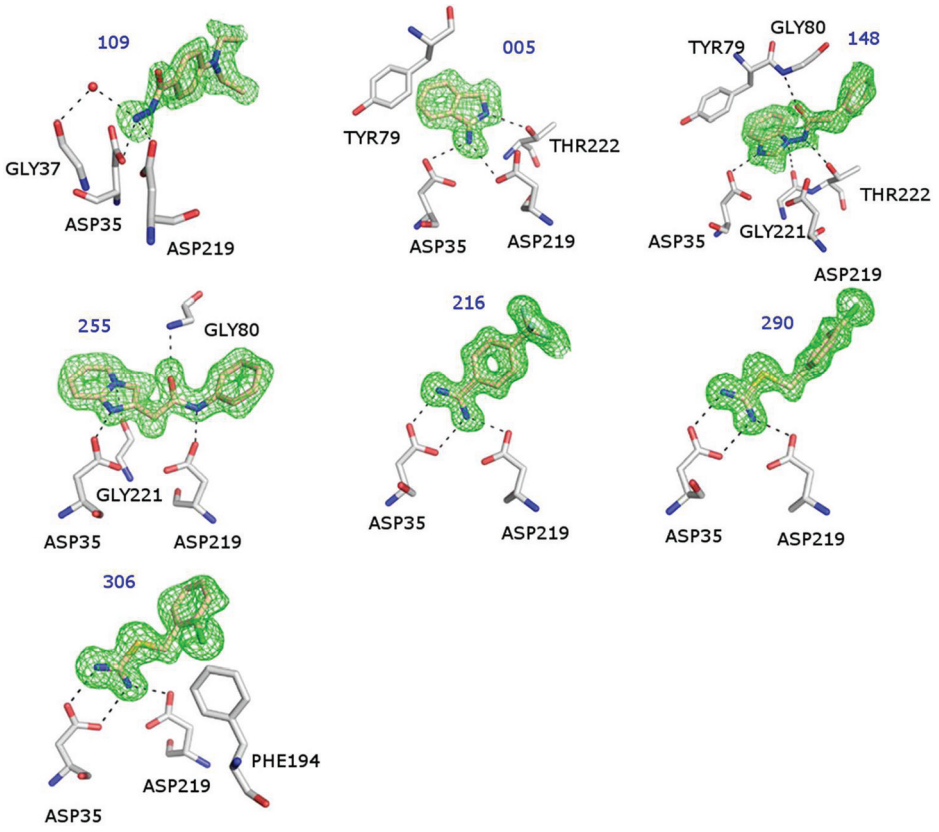

Figure 4. Seven crystal structures that directly interact with the two catalytic aspartates. Nitrogen atoms are in blue, oxygen atoms in red, ligand carbon atoms in salmon, and protein carbons in white. The green mesh shows the $F_o - F_c$ difference electron density at $\sigma = 2.0$.

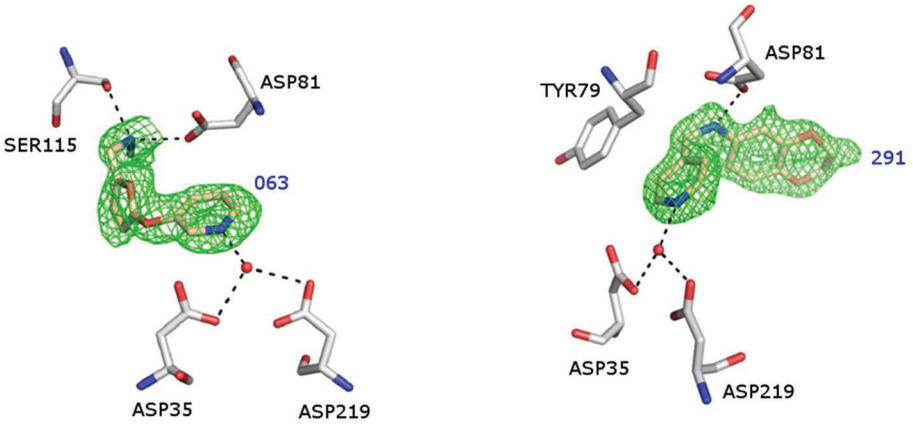

Figure 5. Two fragments interacting with the catalytic aspartates by an interstitial water molecule. Nitrogen atoms are in blue, oxygen atoms in red, ligand carbon atoms in salmon, and protein carbons in white. $F_o - F_c$ difference electron density at $\sigma = 2.0$.

hydrogen bond to Thr222 of the S2 pocket. The fused aromatic benzene ring is located in the S1 pocket, performing a π stacking with Tyr79 (Figure 4). In the case of the aspartyl protease BACE, a ligand skeleton of similar topology has been described as binding chemotype.[58]

Although fragments **148** and **255** are chemically similar, their binding modes show interesting differences. **148** interacts only with one of the catalytic aspartates (Asp35). In addition, a hydrogen bond to Thr222 and to Gly221 is formed. Furthermore, this fragment forms via the carbonyl oxygen of the amide group, an H-bond to the NH group of Gly80. Its benzimidazole moiety occupies the S1 pocket, while the phenyl ring at the opposite end is orientated toward the S2 pocket. **255** binds above the catalytic dyad, forming hydrogen bonds to both aspartates, another hydrogen bond is experienced via its carbonyl amide group toward the flap addressing Gly80. The larger fused 5−6 ring system occupies the S1 pocket similar to the binding mode of **148**. While **148** is addressing the S2 pocket, in this case the phenyl ring is pointing toward the S1′ pocket (Figure 4).

Fragments **216**, **306**, and **290** form the three most likely salt-type hydrogen bonds toward the catalytic dyad by placing an amidine group next to the two aspartates (Figure 4). All prefer a paired double hydrogen bond with Asp35, whereas Asp219 is only addressed via one single H-bond contact. It is difficult to speculate on the most likely protonation state of the dyad

dx.doi.org/10.1021/jm200642w | J. Med. Chem. 2011, 54, 7784–7796

regarding the observed binding mode.[59] Usually Asp35 is assumed to be fully deprotonated whereas Asp 219 should carry one proton. Interestingly, for β-secretase a complex with an amidine derivative similar to **306** and **290** has been reported but with reverse orientation (PDB code 3KMX).[48] Nevertheless, the distances across the catalytic dyad in β-secretase are somewhat larger than in endothiapepsin, which might (with some care) explain the deviating binding properties observed in the former protease. The aromatic portions of the inhibitors are positioned in front of the S1′ pocket. **306** and **290** vary only in the position of the attached chlorine. While the para-attached chlorine in **290** is pointing into the surrounding solvent environment, the ortho-substituent in **306** enables the chlorine to interact with Phe194. Here, the chlorine atom is pointing with about 4 Å distance toward the plane of the Phe194 phenyl ring. This geometry departs somewhat from the ideal interaction pattern described for chlorine−aromatic ring system contacts. In the structure of **216** an additional DMSO molecule is found exactly at the same position as in the complex with **109**.

Binding mediated via a water molecule can be observed for **63** and **291** (Figure 5). In both cases, the catalytic water molecules bridge an interaction between a pyridine-type nitrogen and the catalytic dyad.

The protein conformation remains unchanged across all 11 crystal structures. Especially the flap region, known to be flexible, is found in close state and varies only slightly between the different structures. Therefore, the fragments bury their surface between 68% (**216**) and 83% (**041**, **109**, and **005**). Similarly, the percentage of the hydrophobic buried surface varies from 67% (**216**) to 93% (**063**). These values were determined using the program MS with a probe radius of 1.4 Å.[60]

Besides the interaction with the catalytic aspartates, **63** forms two hydrogen bonds with its secondary amino group at the opposite end of the fragment. The functional group is positioned between the flap aspartate (Asp81) and Ser115. The central part of the fragment binds to the S1 pocket.

291 also addresses Asp81 with a nitrogen. The pyridine ring is able to perform a π-stacking with Tyr79. The benzdioxane moiety reaches into the S3 pocket.

41 and **284** show no direct or supposedly very weak and extended interactions with the two aspartates of the catalytic dyad (Figure 6). **41** interacts with the flap residues by forming two hydrogen bonds, one through the hydrogen at the piperidine nitrogen to the terminal carboxylate group of Asp81 and one via its amide carbonyl to the backbone NH group of the same residue. The adjacent amide nitrogen forms a hydrogen bond toward Thr222 in front of the S2 pocket. The aromatic piperonyl ring system is pointing toward the S1′ pocket, whereas the hydrophobic portion of the piperidine ring occupies the S1 pocket.

284 forms hydrogen bonds via its hydroxyl function to the backbone nitrogen of Gly80 of the flap and via its pyrrolidine nitrogen to Gly221 at the bottom of the binding pocket. As this pyrrolidine nitrogen is most likely protonated under the acidic buffer conditions applied for soaking, a second rather long H-bond contact (3.5 Å) is formed to the water molecule hosted at the pivot between both aspartates of the catalytic dyad. The hydrophobic portion of the pyrrolidine moiety occupies the S1 pocket, while the opposing aromatic ring is orientated toward the S2 pocket.

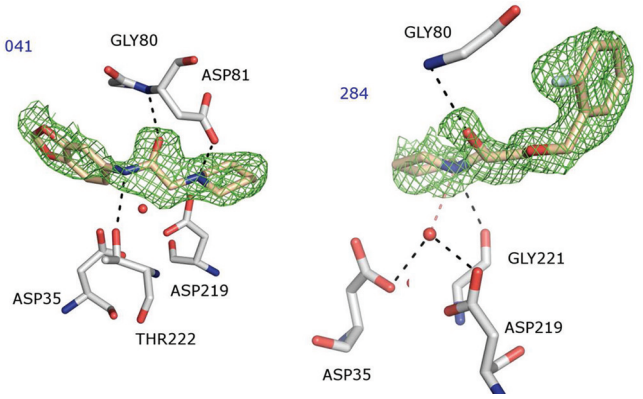

Figure 6. Fragments showing no direct interaction to the two aspartates. Nitrogen atoms are in blue, oxygen atoms in red, ligand carbon atoms in salmon, and protein carbons in white. $F_o - F_c$ difference electron density at $\sigma = 2.0$.

The different electron densities of **41** and **284** are less well-defined compared to the other nine fragments, indicating a rather large residual mobility of the fragments in the binding pocket. Probably this observation is due to the fact that these fragments are not in direct contact with the strongly fixed, most likely negatively charged catalytic dyad.

An overlay of all crystal structures is shown in Figure 7 and Figure 8. Almost the entire volume of the various subpockets of

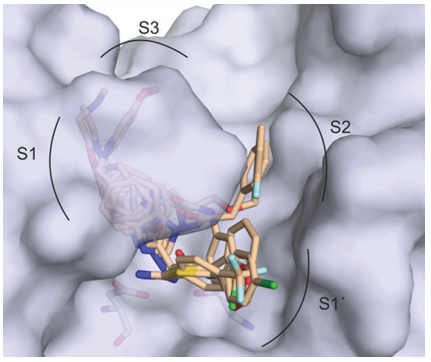

Figure 7. Overlay of all 11 fragment structures. The binding pocket is in surface representation, and specificity pockets are indicated. Carbon atoms are colored in salmon, nitrogen in blue, oxygen in red, chlorine in green, and fluorine in cyan.

this protease is occupied by the different fragments. Besides binding to the catalytic dyad, several preferred interactions can be observed. The following interactions highlight some of these contacts. Seven compounds (**005**, **041**, **148**, **255**, **284**, **291**, and **109**) orientate a hydrophobic ligand portion toward the S1 pocket. A ligand carbonyl group addressing the backbone nitrogen of the flap aspartate is observed in three cases (**041**, **148**, **284**). Thr222 at the bottom of the binding pocket is addressed by an NH functionality of **005** and **148**. Remarkably, all these interactions are also observed for pepstatin, a well-known highly potent inhibitor of most aspartic proteases not designed by a medicinal chemistry program but optimized by microorganisms using principles of evolution.

Although the most prominent interactions with the protein are also experienced by known inhibitors such as pepstatin, our fragment screen affords seven new interaction patterns with the

dx.doi.org/10.1021/jm200642w | J. Med. Chem. 2011, 54, 7784–7796

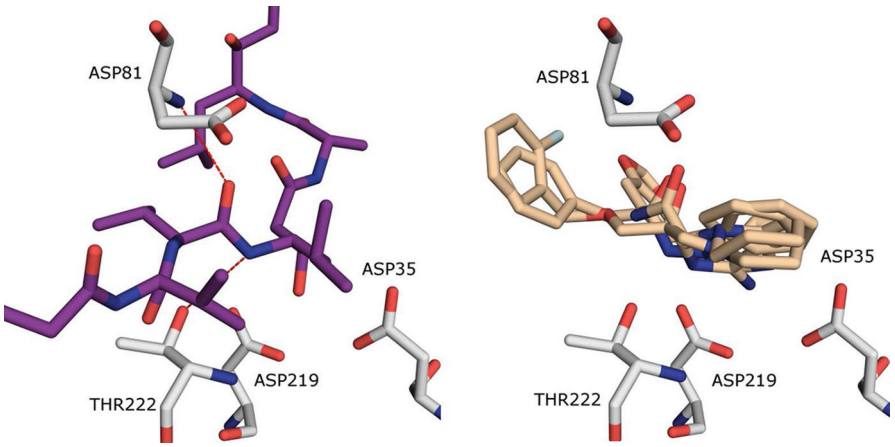

Figure 8. Overlay of four fragments (light brown) (right) and pepstatin (purple) (left). The flap aspartate and Thr222 are shown in white. Two interactions performed by pepstatin are marked with dashed lines.

catalytic dyad not reported previously for pepsin-like aspartic proteinases.

A closer inspection of the binding poses suggests several ways to replace active-site water molecules. While in four of our structures the catalytic water molecule is displaced by a most likely charged nitrogen, the disordered water molecules found in the S2 and S1′ pockets are substituted by hydrophobic ligand portions. A water molecule found between Asp81, Ser83, and Ser115 is not directly substituted but displaced by a secondary nitrogen (**063** or **284**) or by a neighboring hydrophobic moiety (**109**). In all fragments comprising an amidine functional group, a water molecule binding to Gly37 is displaced by the second nitrogen atom interacting with the oxygen atom of Asp35 being more exposed to the binding site.

DISCUSSION

The fluorescence-based assay screening results and the obtained crystal structures with endothiapepsin suggest that the library has been convincingly well designed for crystallographic fragment screening, bearing in mind that this library was assembled for all kinds of targets and not specifically for aspartyl proteases. Nevertheless, this conclusion is preliminary and based on the result of one single target, for which we obtained 11 crystal structures out of the 364-membered library. In this context it is worth mentioning that one of our industry partners in the project screened the library for the phophodiesterase PDE4 and found eight hits and for the CHK1 kinase four hits (D. Ullmann, T. Neuefeind, Proteros GmbH Munich, Germany, personal communication).

The solubility of the fragments in the assembled library is very promising and emphasizes the importance of this property, as 66% of the compounds showed at least a solubility of 1.5 mmol/L and 76% are at least soluble at 1 mmol/L. This criterion is critical for success because fragments are weak binders and therefore have to be applied in rather high concentrations for crystallization and assay experiments.

As indicated earlier, the library design was not consistent with the "RO3" of Astex. The assembled compounds are in agreement with these rules with respect to molecular weight, log *P*, and the TPSA. However, we cover a larger range concerning the number of hydrogen-bond donors and in particular acceptors and in the number of free rotatable bonds. If we had designed a library strictly within the limitations of the "RO3", we would have missed seven fragments of our detected hits for endothiapepsin. Particularly remarkable is the fact that all four remaining crystallographically confirmed fragments have amidine-like moieties and are in agreement with the rules. However, with respect to drug design and medicinal chemistry follow-up programs, they would provide a rather narrow range of chemotypes. Clearly, a research study applying fragment-based lead discovery expects a much broader range of chemical diversity. Therefore, the strict threshold of less than three donors and acceptors and the number of rotatable bonds is questionable.

With respect to fragment growing and fragment merging a sufficient number of synthetically accessible functional groups is of utmost importance for subsequent chemical synthesis. Alleviating these criteria enlarges the available fragment pool and potentially leads to higher hit rates of binding fragments suitable for further ligand design. As a matter of fact usually the functional groups are motifs that show hydrogen-bond donor or hydrogen-bond acceptor properties.

CONCLUSION

The suitability of a fragment library for successful crystallization and follow-up optimization is not only determined by the library design. The correct choice of the experimental screening conditions is equally essential to discover reasonable hits. The first step is usually a screening assay followed by a crystallographic hit validation. In our case, we have chosen a functional assay at 1 mmol/L compound concentration and demanded at least 40% protein inhibition. On the one hand, this criterion was quite successful, as we were able to determine 11 crystal structures out of 55 assay hits. On the other hand, it is remarkable that according to our crystallographic screening results, no obvious correlation between potency observed in the assay and probability to receive a crystal structure can be established. It might even be possible that there are still some compounds with an even lower inhibition rate that would penetrate into the crystals and disclose their successful binding in a crystal structure. Picking fragments according to positive assay results seems indicative but by no means reliable. In the literature several protocols have been reported as screening strategies which were based on techniques such as SPR, NMR, biochemical functional assay, mass spectrometry, and replacement titration experiments. Interestingly, hit lists were generated showing sometimes minimal overlap. The physical bases for these observations are still rather unclear. However,

dx.doi.org/10.1021/jm200642w|*J. Med. Chem.* 2011, 54, 7784–7796

Table 5. Crystallographic Data (Part 1)

parameter	bound fragment, PDB code					
	109, 3PBZ	**005**, 3PBD	**148**, 3PMY	**255**, 3PM4	**216**, 3PCW	**290**, 3PLD
	Data Collection and Processing					
collection site	BL 14.2	in-house	BL 14.2	in-house	BL 14.2	BL 14.3
λ (Å)	0.918 41	1.541 78	0.918 41	1.541 78	0.918 41	0.894 40
space group	$P2_1$	$P2_1$	$P2_1$	$P2_1$	$P2_1$	$P2_1$
unit cell parameters						
a (Å)	45.1	45.3	45.4	45.2	45.3	45.3
b (Å)	73.3	73.1	73.1	73.5	73.1	73.0
c (Å)	52.4	52.7	52.8	52.5	52.5	52.8
β (deg)	109.2	109.8	109.6	109.2	109.5	109.6
resoln (Å)	30−1.48	30−1.70	30−1.38	40−1.68	20−1.25	40−1.40
highest resoln shell	1.51−1.48	1.73−1.70	1.40−1.38	1.71−1.68	1.27−1.25	1.42−1.40
unique reflns	51 357	35 536	65 186	37 129	86 999	63 118
R_{sym} (%)[a]	5.8 (25.5)	4.6 (20.8)	4.6 (21.9)	4.1 (21.2)	3.6 (18.9)	5.9 (33.0)
completeness (%)[a]	95.5 (86.0)	99.5 (99.3)	97.7 (87.5)	100 (100)	98.0 (84.5)	99.3 (97.6)
redundancy[a]	2.7 (2.0)	2.8 (2.6)	3.0 (2.0)	3.9 (3.6)	3.6 (2.1)	3.1 (2.6)
I/σ[a]	15.9 (2.7)	29.4 (4.7)	22.1 (3.8)	31.4 (6.0)	27.9 (3.9)	18.5 (2.4)
	Refinement					
final R_{free}	17.9	19.6	16.2	19.3	15.0	16.6
final R_{work}	12.8	15.3	12.2	15.3	11.6	12.9
no. of water molecules	260	323	292	303	304	300
Ramachandran plot						
most favored regions (%)	94.2	92.8	94.6	93.9	93.5	94.6
additional allowed regions (%)	5.8	7.2	5.4	6.1	6.5	5.4
mean B factors (Å^2)						
protein atoms	14.2	16.3	11.4	16.5	12.0	13.0
water molecules	27.7	28.7	25.4	28.4	26.3	26.7
ligand (fragment)	28.3	28.6	31.0	20.5	21.5	23.7
ligand (other)[b]	27.6	24.4	17.5	25.0	24.3	19.9
rmsd bond length (Å)	0.009	0.007	0.011	0.008	0.013	0.010
rmsd bond angle (deg)	2.7	2.4	2.7	2.5	2.8	2.7

[a]Values in parentheses are for the highest resolution shell. [b]Other ligands are glycerol and/or DMSO.

structure-based fragment lead discovery needs a well-resolved structure as an entry point into a medicinal chemistry follow-up program. Usually this is a crystal structure. Thus, the final consequence of these observations might be to perform fragment screening primarily on protein crystals, a perspective presently not followed as the X-ray facilities would have to be expanded and adapted to this strategy. Most setups are yet not suited for this concept and would require further automation and more frequent access to synchrotron beam time. We also refrained up to now from such attempts, as it appears only feasible with the required automation and approved access to synchrotron beam time to include all 364 library fragments in the screening process.

Nevertheless, in this project 11 crystal structures with a fragment bound to endothiapepsin could be determined. These fragments show diverse binding modes filling up almost the entire volume of the various specificity pockets. They can be divided into three different categories which include direct contacts to the catalytic aspartates, binding mediated by a water molecule, and no direct binding to the catalytic dyad. The various binding modes provide novel ideas to address the active site of aspartic proteases. The fragment structures are also suitable to elucidate experimentally the hot spots of binding. An alignment of all structures enables us to "map out" possible interaction patterns and binding motifs with the protease. Remarkably, pepstatin, a potent nonselective aspartyl protease inhibitor, uses prominent interactions highlighted by our fragments to achieve potent binding.

MATERIALS AND METHODS

Inhibition Assay. Endothiapepsin was purified from Suparen (provided by DSM Food Specialties) by exchanging the buffer to 0.1 M acetate buffer, pH 4.6, using a Vivaspin 20 with a molecular weight cutoff at 10 000 Da. The protein concentration was measured by absorbance at 280 nm assuming an extinction coefficient of 1.15 for 1 mg/mL solutions.[61]

A 100 mM stock solution in DMSO was prepared for all compounds of the fragment library. Because of solubility reasons in 18 cases, only 50 mM could be achieved. Fourteen compounds were not soluble in DMSO and therefore excluded from the screen. As substrate we used Abz-Thr-Ile-Nle-p-nitro-Phe-Gln-Arg-NH_2 (purchased from Bachem). The assay was performed with a Tecan Safire^{2}microplate reader at an excitation wavelength of 337 nm and an emission wavelength of 414 nm. The K_m of the substrate toward endothiapepsin was determined to 1.6 μM. The assay buffer (0.1 M acetate buffer, pH 4.6, containing 0.01% Tween 20) was premixed with the substrate and the screening compound, whereas the protein was added directly before measurement. The final reaction volume was 200 μM containing 4 nM endothiapepsin, 1.8 μM substrate, and 1 mM test compound (or 500 μM in the cases where a 50 mM stock solution was

dx.doi.org/10.1021/jm200642w|J. Med. Chem. 2011, 54, 7784−7796

Table 6. Crystallographic Data (Part 2)

parameter	bound fragment, PDB code				
	306, 3PLL	**63**, 3PB5	**291**, 3PI0	**41**, 3PGI	**284**, 3PMU
Data Collection and Processing					
collection site	BL 14.3	in-house	BL 14.3	in-house	BL 14.2
λ (Å)	0.894 40	1.541 78	0.894 40	1.541 78	0.918 41
space group	$P2_1$	$P2_1$	$P2_1$	$P2_1$	$P2_1$
unit cell parameters					
a (Å)	45.2	45.3	45.3	45.3	45.2
b (Å)	73.1	73.0	73.0	72.8	73.7
c (Å)	52.7	52.5	52.7	52.8	52.5
β (deg)	109.6	109.5	109.4	109.6	109.3
resoln (Å)	40−1.73	30−1.90	40−1.64	30−1.90	20−1.43
highest resoln shell	1.76−1.73	1.93−1.90	1.67−1.64	1.93−1.90	1.45−1.43
unique reflns	32 328	25 453	38 684	25 348	59 547
R_{sym} (%)[a]	7.2 (34.7)	7.2 (30.0)	5.3 (33.3)	6.5 (28.7)	7.3 (42.9)
completeness (%)[a]	96.4(94.7)	100(99.6)	98.0(97.2)	99.2(96.0)	99.4(98.2)
redundancy[a]	3.1 (2.8)	4.0 (3.6)	3.0 (2.6)	3.6 (3.2)	3.1 (2.7)
I/σ [a]	13.2 (2.6)	19.0 (4.1)	20.4 (3.0)	26.7 (4.3)	14.3 (2.3)
Refinement					
final R_{free}	22.0	22.2	18.4	21.5	18.9
final R_{work}	16.3	16.1	15.1	16.2	16.5
no. of water molecules	236	237	254	239	264
Ramachandran plot					
most favored regions (%)	93.1	92.8	94.2	93.1	93.9
additional allowed regions (%)	6.9	7.2	5.8	6.9	6.1
mean B factors (Å^2)					
protein atoms	14.8	17.1	13.0	21.4	13.7
water molecules	24.9	27.5	25.4	30.6	24.5
ligand (fragment)	18.2	30.8	25.5	46.0	32.9
ligand (other)[b]	22.3	32.2	24.8	40.4	
rmsd bond length (Å)	0.007	0.006	0.008	0.006	0.005[c]
rmsd bond angle (deg)	2.4	2.2	2.5	2.2	1.1[c]

[a]Values in parentheses are for the highest resolution shell. [b]Other ligands are glycerol and/or DMSO. [c]Low values are due to stronger geometrical restrains used in PHENIX compared to SHELXL.

used). Blanks were prepared in the same way using DMSO instead of the compound stock solution. During measurement the fluorescence increased because of substrate cleavage. For data analysis the initial slope of the fluorescence in the compound containing wells were compared to the initial slope of the blanks. Each compound was measured twice. The final result represents the average of both measurements.

Crystallization and Structure Determination. Crystals of unbound endothiapepsin were grown similarly as described previously.[51] We used the sitting drop vapor diffusion method and a crystallization temperature of 16 °C. The drops contained 2 μL of protein solution (5 mg/mL) and 2 μL of mother liquor. The reservoir solution consisted of 1 mL of 0.1 M NH_4Ac, 0.1 M acetate buffer, pH 4.6, and 26% PEG 4000. Crystals were ready for soaking after about 2 weeks. For each compound, a 1 M stock solution in DMSO was prepared. The crystals were soaked 1−2 days in reservoir buffer containing 25% glycerol and a mixture of two compounds, each at a final concentration of 50 mM. To ensure a clear identification of the bound fragment, the two compounds were chosen by maximal chemical shape diversity. If the compound precipitated, the deposit was ignored. After soaking, the crystals were flash-frozen in liquid nitrogen. If one compound of a cocktail showed binding, the other one was subsequently soaked again in a different mixture or separately. **109** was soaked alone for practical reasons. In two cases (**255**, **148**) the bound compound was soaked again because the difference density was not sufficient for placement of the fragment. These compounds were soaked without an additional fragment. In both cases the difference electron density improved significantly.

In-house data sets were collected on a sealed Cu fine focus X-ray device using a MAR345 image plate. Synchrotron data sets were collected at BESSY beamline 14.2 or 14.3 in Berlin. Bessy beamline 14.2 provides a Rayonix MX-255 CCD detector, beamline 14.3 a Rayonix SX-165mm CCD detector. All data sets were collected at 100 K and processed using HKL2000. Details about the data collection and data reduction are listed in Tables 5 and 6.[62]

The structures were determined by molecular replacement using the program Phaser.[63] Search model was the 0.9 Å structure of endothiapepsin bound to a short peptide (PDB code 1OEW). For cross-validation of the refinement 5% of the reflections were chosen at random for inclusion in the R_{free} set. After initial simulated annealing with CNS, refinement was done using SHELXL.[64] During the last cycles of refinement of the structures containing **109**, **148**, **216**, and **290**, anisotropic refinement was applied. The structure containing fragment **284** was refined using PHENIX.[65] After each cycle the models were inspected and subsequently improved using Coot.[66] In most structures some unexplained difference density remained after refinement. This additional density which also occurred in the binding pocket is probably due to the high amount of soaked compound leading to unspecific binding. It is also possible that this indicates some DMSO molecules showing limited occupancy, as only in two structures fully occupied DMSO molecules could be assigned. To determine the $F_o - F_c$ difference electron density next to the binding pocket (shown in all figures), the fragments have been removed from

dx.doi.org/10.1021/jm200642w|J. Med. Chem. 2011, 54, 7784−7796

the structural models and after additional cycles of refinement the maps were generated.

Solubility Assay. A 500 μM buffered compound solution is prepared using a 10 mM compound stock solution in DMSO. This solution is transferred into three wells (100 μL/well, triplicates) of a 96-well filtration plate (Millipore; 0.2 μm, hydrophilic PVDF, Durapore-MSGVN2250) and incubated at room temperature for 90 min while agitating at 100 rpm (sample wells). In parallel the same solution is transferred into three wells (100 μL/well, triplicate) of a 96-well, UV transparent plate (Greiner, no. 655801) prefilled with 100 μL/well acetonitrile, thereby ensuring complete dissolution of the compounds (control wells). In order to separate the precipitate from dissolved compound, the filtration plate is centrifuged (2000 rpm, 5 min, room temperature). The filtrates are collected directly in the wells of the UV transparent plate. After addition of 100 μL/well acetonitrile to the filtrate wells, absorbance spectra are taken (250−500 nm). Spectra of the sample and control wells are integrated and averaged over the triplicates. Kinetic solubility is calculated by 500 μM × (integral sample wells/integral control wells).

■ ASSOCIATED CONTENT

Accession Codes

[†]The PDB accession codes of crystal structures in this contribution are as follows: 3PBZ, 3PBD, 3PMY, 3PM4, 3PCW, 3PLD, 3PLL, 3PB5, 3PI0, 3PGI, 3PMU.

■ AUTHOR INFORMATION

Corresponding Author

*Phone: + 49 6421 282 1313. E-mail: klebe@mailer.uni-marburg.de.

Author Contributions

[#]These authors contributed equally.

■ ACKNOWLEDGMENTS

The present study was funded by the German Minister of Science and Education in the BioChancePlus Program (Project FragScreen No. 0315161C). Financial support is gratefully acknowledged. We thank the support staff at Helmholtz Zentrum Berlin, BESSY II, for their help with the synchrotron data collection, and we thank the German Minister of Science and Education (Grant 05 ES3XBA/5) for financing the travel costs to BESSY II.

■ ABBREVIATIONS USED

NMR, nuclear magnetic resonance; SPR, surface plasmon resonance; RO5, Lipinski's rule of 5; RO3, Astex's rule of 3; DMSO, dimethylsulfoxide; PDB, Protein Data Bank; TPSA, total polar surface area

■ REFERENCES

(1) Lipinski, C. A.; Lombardo, F.; Dominy, B. W.; Feeney, P. J. Experimental and computational approaches to estimate solubility and permeability in drug discovery and development settings. *Adv. Drug Delivery Rev.* **2001**, *46*, 3−26.

(2) Abad-Zapatero, C.; Metz, J. T. Ligand efficiency indices as guideposts for drug discovery. *Drug Discovery Today* **2005**, *10*, 464−469.

(3) Blundell, T. L.; Patel, S. High-throughput X-ray crystallography for drug discovery. *Curr. Opin. Pharmacol.* **2004**, *4*, 490−496.

(4) Hartshorn, M. J.; Murray, C. W.; Cleasby, A.; Frederickson, M.; Tickle, I. J.; Jhoti, H. Fragment-based lead discovery using X-ray crystallography. *J. Med. Chem.* **2005**, *48*, 403−413.

(5) Tickle, I.; Sharff, A.; Vinkovic, M.; Yon, J.; Jhoti, H. High-throughput protein crystallography and drug discovery. *Chem. Soc. Rev.* **2004**, *33*, 558−565.

(6) Dalvit, C.; Fasolini, M.; Flocco, M.; Knapp, S.; Pevarello, P.; Veronesi, M. NMR-based screening with competition water-ligand observed via gradient spectroscopy experiments: detection of high-affinity ligands. *J. Med. Chem.* **2002**, *45*, 2610−2614.

(7) Fejzo, J.; Lepre, C. A.; Peng, J. W.; Bemis, G. W.; Ajay.; Murcko, M. A.; Moore, J. M. The SHAPES strategy: an NMR-based approach for lead generation in drug discovery. *Chem. Biol.* **1999**, *6*, 755−769.

(8) Shuker, S. B.; Hajduk, P. J.; Meadows, R. P.; Fesik, S. W. Discovering high-affinity ligands for proteins: SAR by NMR. *Science* **1996**, *274*, 1531−1534.

(9) Blundell, T. L.; Jhoti, H.; Abell, C. High-throughput crystallography for lead discovery in drug design. *Nat. Rev. Drug Discovery* **2002**, *1*, 45−54.

(10) Congreve, M.; Carr, R.; Murray, C.; Jhoti, H. A "rule of three" for fragment-based lead discovery? *Drug Discovery Today* **2003**, *8*, 876−877.

(11) Congreve, M.; Aharony, D.; Albert, J.; Callaghan, O.; Campbell, J.; Carr, R. A.; Chessari, G.; Cowan, S.; Edwards, P. D.; Frederickson, M.; McMenamin, R.; Murray, C. W.; Patel, S.; Wallis, N. Application of fragment screening by X-ray crystallography to the discovery of aminopyridines as inhibitors of beta-secretase. *J. Med. Chem.* **2007**, *50*, 1124−1132.

(12) de Kloe, G. E.; Bailey, D.; Leurs, R.; de Esch, I. J. Transforming fragments into candidates: small becomes big in medicinal chemistry. *Drug Discovery Today* **2009**, *14*, 630−646.

(13) Erlanson, D. A. Fragment-based lead discovery: a chemical update. *Curr. Opin. Biotechnol.* **2006**, *17*, 643−652.

(14) Erlanson, D. A.; McDowell, R. S.; O'Brien, T. Fragment-based drug discovery. *J. Med. Chem.* **2004**, *47*, 3463−3482.

(15) Hann, M. M.; Leach, A. R.; Harper, G. Molecular complexity and its impact on the probability of finding leads for drug discovery. *J. Chem. Inf. Comput. Sci.* **2001**, *41*, 856−864.

(16) Jhoti, H. A new school for screening. *Nat. Biotechnol.* **2005**, *23*, 184−186.

(17) Keseru, G. M.; Makara, G. M. Hit discovery and hit-to-lead approaches. *Drug Discovery Today* **2006**, *11*, 741−748.

(18) Leach, A. R.; Hann, M. M.; Burrows, J. N.; Griffen, E. J. Fragment screening: an introduction. *Mol. BioSyst.* **2006**, *2*, 430−446.

(19) Makara, G. M. On sampling of fragment space. *J. Med. Chem.* **2007**, *50*, 3214−3221.

(20) Rees, D. C.; Congreve, M.; Murray, C. W.; Carr, R. Fragment-based lead discovery. *Nat. Rev. Drug Discovery* **2004**, *3*, 660−672.

(21) Zartler, E. R.; Shapiro, M. J. Fragonomics: fragment-based drug discovery. *Curr. Opin. Chem. Biol.* **2005**, *9*, 366−370.

(22) Hajduk, P. J. Puzzling through fragment-based drug design. *Nat. Chem. Biol.* **2006**, *2*, 658−659.

(23) Barker, J. J.; Barker, O.; Courtney, S. M.; Gardiner, M.; Hesterkamp, T.; Ichihara, O.; Mather, O.; Montalbetti, C. A.; Muller, A.; Varasi, M.; Whittaker, M.; Yarnold, C. J. Discovery of a novel Hsp90 inhibitor by fragment linking. *ChemMedChem* **2010**, *5*, 1697−1700.

(24) Brough, P. A.; Aherne, W.; Barril, X.; Borgognoni, J.; Boxall, K.; Cansfield, J. E.; Cheung, K. M.; Collins, I.; Davies, N. G.; Drysdale, M. J.; Dymock, B.; Eccles, S. A.; Finch, H.; Fink, A.; Hayes, A.; Howes, R.; Hubbard, R. E.; James, K.; Jordan, A. M.; Lockie, A.; Martins, V.; Massey, A.; Matthews, T. P.; McDonald, E.; Northfield, C. J.; Pearl, L. H.; Prodromou, C.; Ray, S.; Raynaud, F. I.; Roughley, S. D.; Sharp, S. Y.; Surgenor, A.; Walmsley, D. L.; Webb, P.; Wood, M.; Workman, P.; Wright, L. 4,5-Diarylisoxazole Hsp90 chaperone inhibitors: potential therapeutic agents for the treatment of cancer. *J. Med. Chem.* **2008**, *51*, 196−218.

(25) Cheung, K. M.; Matthews, T. P.; James, K.; Rowlands, M. G.; Boxall, K. J.; Sharp, S. Y.; Maloney, A.; Roe, S. M.; Prodromou, C.; Pearl, L. H.; Aherne, G. W.; McDonald, E.; Workman, P. The identification, synthesis, protein crystal structure and in vitro biochemical evaluation of a new 3,4-diarylpyrazole class of Hsp90 inhibitors. *Bioorg. Med. Chem. Lett.* **2005**, *15*, 3338−3343.

(26) Dymock, B. W.; Barril, X.; Brough, P. A.; Cansfield, J. E.; Massey, A.; McDonald, E.; Hubbard, R. E.; Surgenor, A.; Roughley, S.

D.; Webb, P.; Workman, P.; Wright, L.; Drysdale, M. J. Novel, potent small-molecule inhibitors of the molecular chaperone Hsp90 discovered through structure-based design. *J. Med. Chem.* **2005**, *48*, 4212−4215.

(27) Huth, J. R.; Park, C.; Petros, A. M.; Kunzer, A. R.; Wendt, M. D.; Wang, X.; Lynch, C. L.; Mack, J. C.; Swift, K. M.; Judge, R. A.; Chen, J.; Richardson, P. L.; Jin, S.; Tahir, S. K.; Matayoshi, E. D.; Dorwin, S. A.; Ladror, U. S.; Severin, J. M.; Walter, K. A.; Bartley, D. M.; Fesik, S. W.; Elmore, S. W.; Hajduk, P. J. Discovery and design of novel HSP90 inhibitors using multiple fragment-based design strategies. *Chem. Biol. Drug Des.* **2007**, *70*, 1−12.

(28) Woodhead, A. J.; Angove, H.; Carr, M. G.; Chessari, G.; Congreve, M.; Coyle, J. E.; Cosme, J.; Graham, B.; Day, P. J.; Downham, R.; Fazal, L.; Feltell, R.; Figueroa, E.; Frederickson, M.; Lewis, J.; McMenamin, R.; Murray, C. W.; O'Brien, M. A.; Parra, L.; Patel, S.; Phillips, T.; Rees, D. C.; Rich, S.; Smith, D. M.; Trewartha, G.; Vinkovic, M.; Williams, B.; Woolford, A. J. Discovery of (2,4-dihydroxy-5-isopropylphenyl)-[5-(4-methylpiperazin-1-ylmethyl)-1,3-dihydroisoindol-2-yl]methanone (AT13387), a novel inhibitor of the molecular chaperone Hsp90 by fragment based drug design. *J. Med. Chem.* **2010**, *53*, 5956−5969.

(29) Caldwell, J. J.; Davies, T. G.; Donald, A.; McHardy, T.; Rowlands, M. G.; Aherne, G. W.; Hunter, L. K.; Taylor, K.; Ruddle, R.; Raynaud, F. I.; Verdonk, M.; Workman, P.; Garrett, M. D.; Collins, I. Identification of 4-(4-aminopiperidin-1-yl)-7*H*-pyrrolo[2,3-*d*]-pyrimidines as selective inhibitors of protein kinase B through fragment elaboration. *J. Med. Chem.* **2008**, *51*, 2147−2157.

(30) Donald, A.; McHardy, T.; Rowlands, M. G.; Hunter, L. J.; Davies, T. G.; Berdini, V.; Boyle, R. G.; Aherne, G. W.; Garrett, M. D.; Collins, I. Rapid evolution of 6-phenylpurine inhibitors of protein kinase B through structure-based design. *J. Med. Chem.* **2007**, *50*, 2289−2292.

(31) Frederickson, M.; Callaghan, O.; Chessari, G.; Congreve, M.; Cowan, S. R.; Matthews, J. E.; McMenamin, R.; Smith, D. M.; Vinkovic, M.; Wallis, N. G. Fragment-based discovery of mexiletine derivatives as orally bioavailable inhibitors of urokinase-type plasminogen activator. *J. Med. Chem.* **2008**, *51*, 183−186.

(32) Medina, J. s. R.; Blackledge, C. W.; Heerding, D. A.; Campobasso, N.; Ward, P.; Briand, J.; Wright, L.; Axten, J. M. Aminoindazole PDK1 inhibitors: a case study in fragment-based drug discovery. *ACS Med. Chem. Lett.* **2010**, *1*, 439−442.

(33) Nordstrom, H.; Gossas, T.; Hamalainen, M.; Kallblad, P.; Nystrom, S.; Wallberg, H.; Danielson, U. H. Identification of MMP-12 inhibitors by using biosensor-based screening of a fragment library. *J. Med. Chem.* **2008**, *51*, 3449−3459.

(34) Saxty, G.; Woodhead, S. J.; Berdini, V.; Davies, T. G.; Verdonk, M. L.; Wyatt, P. G.; Boyle, R. G.; Barford, D.; Downham, R.; Garrett, M. D.; Carr, R. A. Identification of inhibitors of protein kinase B using fragment-based lead discovery. *J. Med. Chem.* **2007**, *50*, 2293−2296.

(35) Tsai, J.; Lee, J. T.; Wang, W.; Zhang, J.; Cho, H.; Mamo, S.; Bremer, R.; Gillette, S.; Kong, J.; Haass, N. K.; Sproesser, K.; Li, L.; Smalley, K. S.; Fong, D.; Zhu, Y. L.; Marimuthu, A.; Nguyen, H.; Lam, B.; Liu, J.; Cheung, I.; Rice, J.; Suzuki, Y.; Luu, C.; Settachatgul, C.; Shellooe, R.; Cantwell, J.; Kim, S. H.; Schlessinger, J.; Zhang, K. Y.; West, B. L.; Powell, B.; Habets, G.; Zhang, C.; Ibrahim, P. N.; Hirth, P.; Artis, D. R.; Herlyn, M.; Bollag, G. Discovery of a selective inhibitor of oncogenic B-Raf kinase with potent antimelanoma activity. *Proc. Natl. Acad. Sci. U.S.A.* **2008**, *105*, 3041−3046.

(36) Wyatt, P. G.; Woodhead, A. J.; Berdini, V.; Boulstridge, J. A.; Carr, M. G.; Cross, D. M.; Davis, D. J.; Devine, L. A.; Early, T. R.; Feltell, R. E.; Lewis, E. J.; McMenamin, R. L.; Navarro, E. F.; O'Brien, M. A.; O'Reilly, M.; Reule, M.; Saxty, G.; Seavers, L. C.; Smith, D. M.; Squires, M. S.; Trewartha, G.; Walker, M. T.; Woolford, A. J. Identification of *N*-(4-piperidinyl)-4-(2,6-dichlorobenzoylamino)-1*H*-pyrazole-3-carboxamide (AT7519), a novel cyclin dependent kinase inhibitor using fragment-based X-ray crystallography and structure based drug design. *J. Med. Chem.* **2008**, *51*, 4986−4999.

(37) Liu, G.; Szczepankiewicz, B. G.; Pei, Z.; Janowick, D. A.; Xin, Z.; Hajduk, P. J.; Abad-Zapatero, C.; Liang, H.; Hutchins, C. W.; Fesik, S. W.; Ballaron, S. J.; Stashko, M. A.; Lubben, T.; Mika, A. K.; Zinker, B. A.; Trevillyan, J. M.; Jirousek, M. R. Discovery and structure−activity relationship of oxalylarylaminobenzoic acids as inhibitors of protein tyrosine phosphatase 1B. *J. Med. Chem.* **2003**, *46*, 2093−2103.

(38) Liu, G.; Xin, Z.; Liang, H.; Abad-Zapatero, C.; Hajduk, P. J.; Janowick, D. A.; Szczepankiewicz, B. G.; Pei, Z.; Hutchins, C. W.; Ballaron, S. J.; Stashko, M. A.; Lubben, T. H.; Berg, C. E.; Rondinone, C. M.; Trevillyan, J. M.; Jirousek, M. R. Selective protein tyrosine phosphatase 1B inhibitors: targeting the second phosphotyrosine binding site with non-carboxylic acid-containing ligands. *J. Med. Chem.* **2003**, *46*, 3437−3440.

(39) Liu, G.; Xin, Z.; Pei, Z.; Hajduk, P. J.; Abad-Zapatero, C.; Hutchins, C. W.; Zhao, H.; Lubben, T. H.; Ballaron, S. J.; Haasch, D. L.; Kaszubska, W.; Rondinone, C. M.; Trevillyan, J. M.; Jirousek, M. R. Fragment screening and assembly: a highly efficient approach to a selective and cell active protein tyrosine phosphatase 1B inhibitor. *J. Med. Chem.* **2003**, *46*, 4232−4235.

(40) Lubbers, T.; Angehrn, P.; Gmunder, H.; Herzig, S. Design, synthesis, and structure−activity relationship studies of new phenolic DNA gyrase inhibitors. *Bioorg. Med. Chem. Lett.* **2007**, *17*, 4708−4714.

(41) Oblak, M.; Grdadolnik, S. G.; Kotnik, M.; Jerala, R.; Filipic, M.; Solmajer, T. In silico fragment-based discovery of indolin-2-one analogues as potent DNA gyrase inhibitors. *Bioorg. Med. Chem. Lett.* **2005**, *15*, 5207−5210.

(42) Sutherland, A. G.; Alvarez, J.; Ding, W.; Foreman, K. W.; Kenny, C. H.; Labthavikul, P.; Mosyak, L.; Petersen, P. J.; Rush, T. S. 3rd; Ruzin, A.; Tsao, D. H.; Wheless, K. L. Structure-based design of carboxybiphenylindole inhibitors of the ZipA-FtsZ interaction. *Org. Biomol. Chem.* **2003**, *1*, 4138−4140.

(43) Swayze, E. E.; Jefferson, E. A.; Sannes-Lowery, K. A.; Blyn, L. B.; Risen, L. M.; Arakawa, S.; Osgood, S. A.; Hofstadler, S. A.; Griffey, R. H. SAR by MS: a ligand based technique for drug lead discovery against structured RNA targets. *J. Med. Chem.* **2002**, *45*, 3816−3819.

(44) Tsao, D. H.; Sutherland, A. G.; Jennings, L. D.; Li, Y.; Rush, T. S. 3rd; Alvarez, J. C.; Ding, W.; Dushin, E. G.; Dushin, R. G.; Haney, S. A.; Kenny, C. H.; Malakian, A. K.; Nilakantan, R.; Mosyak, L. Discovery of novel inhibitors of the ZipA/FtsZ complex by NMR fragment screening coupled with structure-based design. *Bioorg. Med. Chem.* **2006**, *14*, 7953−7961.

(45) Bruncko, M.; Oost, T. K.; Belli, B. A.; Ding, H.; Joseph, M. K.; Kunzer, A.; Martineau, D.; McClellan, W. J.; Mitten, M.; Ng, S. C.; Nimmer, P. M.; Oltersdorf, T.; Park, C. M.; Petros, A. M.; Shoemaker, A. R.; Song, X.; Wang, X.; Wendt, M. D.; Zhang, H.; Fesik, S. W.; Rosenberg, S. H.; Elmore, S. W. Studies leading to potent, dual inhibitors of Bcl-2 and Bcl-xL. *J. Med. Chem.* **2007**, *50*, 641−662.

(46) Edwards, P. D.; Albert, J. S.; Sylvester, M.; Aharony, D.; Andisik, D.; Callaghan, O.; Campbell, J. B.; Carr, R. A.; Chessari, G.; Congreve, M.; Frederickson, M.; Folmer, R. H.; Geschwindner, S.; Koether, G.; Kolmodin, K.; Krumrine, J.; Mauger, R. C.; Murray, C. W.; Olsson, L. L.; Patel, S.; Spear, N.; Tian, G. Application of fragment-based lead generation to the discovery of novel, cyclic amidine beta-secretase inhibitors with nanomolar potency, cellular activity, and high ligand efficiency. *J. Med. Chem.* **2007**, *50*, 5912−5925.

(47) Murray, C. W.; Callaghan, O.; Chessari, G.; Cleasby, A.; Congreve, M.; Frederickson, M.; Hartshorn, M. J.; McMenamin, R.; Patel, S.; Wallis, N. Application of fragment screening by X-ray crystallography to beta-secretase. *J. Med. Chem.* **2007**, *50*, 1116−1123.

(48) Wang, Y. S.; Strickland, C.; Voigt, J. H.; Kennedy, M. E.; Beyer, B. M.; Senior, M. M.; Smith, E. M.; Nechuta, T. L.; Madison, V. S.; Czarniecki, M.; McKittrick, B. A.; Stamford, A. W.; Parker, E. M.; Hunter, J. C.; Greenlee, W. J.; Wyss, D. F. Application of fragment-based NMR screening, X-ray crystallography, structure-based design, and focused chemical library design to identify novel microM leads for the development of nM BACE-1 (beta-site APP cleaving enzyme 1) inhibitors. *J. Med. Chem.* **2010**, *53*, 942−950.

(49) Coates, L.; Tuan, H. F.; Tomanicek, S.; Kovalevsky, A.; Mustyakimov, M.; Erskine, P.; Cooper, J. The catalytic mechanism of an aspartic proteinase explored with neutron and X-ray diffraction. *J. Am. Chem. Soc.* **2008**, *130*, 7235−7237.

(50) Cooper, J.; Quail, W.; Frazao, C.; Foundling, S. I.; Blundell, T. L.; Humblet, C.; Lunney, E. A.; Lowther, W. T.; Dunn, B. M. X-ray crystallographic analysis of inhibition of endothiapepsin by cyclohexyl renin inhibitors. *Biochemistry* **1992**, *31*, 8142−8150.
(51) Geschwindner, S.; Olsson, L. L.; Albert, J. S.; Deinum, J.; Edwards, P. D.; de Beer, T.; Folmer, R. H. Discovery of a novel warhead against beta-secretase through fragment-based lead generation. *J. Med. Chem.* **2007**, *50*, 5903−5911.
(52) Baurin, N.; Aboul-Ela, F.; Barril, X.; Davis, B.; Drysdale, M.; Dymock, B.; Finch, H.; Fromont, C.; Richardson, C.; Simmonite, H.; Hubbard, R. E. Design and characterization of libraries of molecular fragments for use in NMR screening against protein targets. *J. Chem. Inf. Comput. Sci.* **2004**, *44*, 2157−2166.
(53) *Molecular Operating Environment (MOE)*, version 2008.11; Chemical Computing Group Inc.: Montreal, Canada; http://www.chemcomp.com.
(54) Kramer, C.; Beck, B.; Clark, T. Insolubility classification with accurate prediction probabilities using a MetaClassifier. *J. Chem. Inf. Model.* **2010**, *50*, 404−414.
(55) Kramer, C.; Heinisch, T.; Fligge, T.; Beck, B.; Clark, T. A consistent dataset of kinetic solubilities for early-phase drug discovery. *ChemMedChem* **2009**, *4*, 1529−1536.
(56) Coates, L.; Erskine, P. T.; Crump, M. P.; Wood, S. P.; Cooper, J. B. Five atomic resolution structures of endothiapepsin inhibitor complexes: implications for the aspartic proteinase mechanism. *J. Mol. Biol.* **2002**, *318*, 1405−1415.
(57) Andreeva, N. S.; Rumsh, L. D. Analysis of crystal structures of aspartic proteinases: on the role of amino acid residues adjacent to the catalytic site of pepsin-like enzymes. *Protein Sci.* **2001**, *10*, 2439−2450.
(58) Stachel, S. J.; Coburn, C. A.; Rush, D.; Jones, K. L.; Zhu, H.; Rajapakse, H.; Graham, S. L.; Simon, A.; Katharine Holloway, M.; Allison, T. J.; Munshi, S. K.; Espeseth, A. S.; Zuck, P.; Colussi, D.; Wolfe, A.; Pietrak, B. L.; Lai, M. T.; Vacca, J. P. Discovery of aminoheterocycles as a novel beta-secretase inhibitor class: pH dependence on binding activity part 1. *Bioorg. Med. Chem. Lett.* **2009**, *19*, 2977−2980.
(59) Coates, L.; Erskine, P. T.; Mall, S.; Gill, R.; Wood, S. P.; Myles, D. A.; Cooper, J. B. X-ray, neutron and NMR studies of the catalytic mechanism of aspartic proteinases. *Eur. Biophys. J.* **2006**, *35*, 559−566.
(60) Connolly, M. L. Analytical molecular surface calculation. *J. Appl. Cyrstallogr.* **1983**, *16*, 548−558.
(61) Larson, M. K.; Whitaker, J. R. *Endothia parasitica* protease. Parameters affecting stability of the rennin-like enzyme. *J. Dairy Sci.* **1970**, *53*, 262−269.
(62) Otwinowski, Z.; Minor, W. Processing of X-ray diffraction data collected in oscillation mode. *Methods Enzymol.* **1997**, *276*, 307−326.
(63) McCoy, A. J.; Grosse-Kunstleve, R. W.; Storoni, L. C.; Read, R. J. Likelihood-enhanced fast translation functions. *Acta Crystallogr., Sect. D: Biol. Crystallogr.* **2005**, *61*, 458−464.
(64) Sheldrick, G. M.; Schneider, T. R. SHELXL: high-resolution refinement. *Methods Enzymol.* **1997**, *277*, 319−343.
(65) Adams, P. D.; Afonine, P. V.; Bunkoczi, G.; Chen, V. B.; Davis, I. W.; Echols, N.; Headd, J. J.; Hung, L. W.; Kapral, G. J.; Grosse-Kunstleve, R. W.; McCoy, A. J.; Moriarty, N. W.; Oeffner, R.; Read, R. J.; Richardson, D. C.; Richardson, J. S.; Terwilliger, T. C.; Zwart, P. H. PHENIX: a comprehensive Python-based system for macromolecular structure solution. *Acta Crystallogr., Sect. D: Biol. Crystallogr.* **2010**, *66*, 213−221.
(66) Emsley, P.; Cowtan, K. Coot: model-building tools for molecular graphics. *Acta Crystallogr., Sect. D: Biol. Crystallogr.* **2004**, *60*, 2126−2132.